Springer

Acta Mechanica Sinica

CrossMark click for updates

• RESEARCH PAPER •

Acta Mech. Sin., Vol.38, 421136 (2022)
https://doi.org/10.1007/s10409-021-09081-x

Modified unified co-rotational framework with beam, shell and brick elements for geometrically nonlinear analysis

Yufei Rong, Qin Sun*, and Ke Liang

School of Aeronautics, Northwestern Polytechnical University, Xi'an 710072, China

Received August 3, 2021; accepted September 7, 2021; published online March 1, 2022

The co-rotational finite element formulation is an attractive technique extending the capabilities of an existing high performing linear element to geometrically nonlinear analysis. This paper presents a modified co-rotational framework, unified for beam, shell, and brick elements. A unified zero-spin criterion is proposed to specify the local element frame, whose origin is always located at the centroid. Utilizing this criterion, a spin matrix is introduced, and the local frame is invariant to the element nodal ordering. Additionally, the projector matrix is redefined in a more intuitive way, which is the derivative of local co-rotational element frame with respect to the global one. Furthermore, the nodal rotation is obtained with pseudo vector and instantaneous rotation, under a high-order accurate transformation. The resulting formulations are achieved in unified expression and thus a series of linear elements can be embedded into the framework. Several examples are presented to demonstrate the efficiency and accuracy of the proposed framework for large displacement analysis.

Geometrically nonlinear analysis, Modified co-rotational framework, Unified zero-spin criterion, Spin matrix, Projector

Citation: Y. Rong, Q. Sun, and K. Liang, Modified unified co-rotational framework with beam, shell and brick elements for geometrically nonlinear analysis, Acta Mech. Sin. **38**, 421136 (2022), https://doi.org/10.1007/s10409-021-09081-x

1. Introduction

Although the total and updated Lagrangian formulations are classical methods for geometrically nonlinear analysis, these methods require complicated element formulations and expensive calculations. The co-rotational finite element formulation is a latest method for handling large rotations but small strains. The key idea of this method is to separate the element rigid body motion from the deformational part of its total motion, utilizing a local frame that continuously translates and rotates with the element. The small deformation can be then captured at the level of local element frame, whereas the geometrical nonlinearity is introduced via the rotation of reference frame. During this generic procedure, existing high performing linear elements are updated rather than introducing new element formulations, which shows its simplicity and efficiency.

As its exceptional benefits for structural problems with arbitrarily large rotations, the co-rotational method has gained more extensive interest in the previous years [1-4]. Beam and shell elements have been widely used to model various modern engineering structures, resulting in useful developments and improvements in finite element technology for nonlinear analysis [5, 6]. In 1986, Rankin and Brogan [7] first introduced the element-independent co-rotation as a general framework for large rotations analysis in three dimensions. To improve the performance of the co-rotational method, Rankin and Nour-Omid [8, 9] later proposed a projector matrix with the property that a consistent internal force vector is invariant under its action. Based on this co-rotational framework, many new beam and shell elements have been developed to solve geometrically nonlinear problems [10-12]. Tang et al. [13] simplified the co-rotation algorithm and considered the warping effect of quadrilateral shell elements. The previous methods have almost exclusively been applied to beams and shells partially for the reason that the rotat-

*Corresponding author. E-mail address: sunqin@nwpu.edu.cn (Qin Sun)
Executive Editor: Xu Guo

ing local element frame is fairly straightforwards defined for beams and shells, which is less obvious for a brick element. Some co-rotational formulation variants were developed for three dimensional brick elements in Refs. [14-16]. In addition, Crisfield and Motia [17] presented a unified framework for solids and shells. However, they implemented a complex formulation to determine the local element frame. Also, the rotations are obtained by first order approximation with less accuracy. Therefore, the main thrust in this work is to develop a unified co-rotational framework with much neater formulation and simpler derivation, which allows the extension to different linear elements with different degrees of freedom.

There are some principal features of the co-rotational method to be outlined. The first one is the treatment of non-commutative large nodal rotations [18]. Rankin and Brogan used pseudo vector [7] and instantaneous rotation [8,9] to extract element rotational degrees of freedom from a new large rotation vector. Felippa and Haugen [19] summarized various normalizations which simplify the associated rotator and spinor. Furthermore, Wang and Sun [20] used the quaternion to store and update the finite rotation during the whole analysis thus avoiding the complicated extraction algorithm. Several parameterizations of the large rotations are summarized and compared with each other in Ref. [21]. The specific choice of the local reference frame in relation to the current deformed element configuration is another major issue. Rankin et al. [7-9] proposed a choice for local element frame, by seeking to fit a plane as closely as possible to the deformed element surface. A term involving the spin of local frame was introduced by Crisfield and Moita [17] to make the local frame invariant to the specified order of the element nodes, which is desirable for extending the co-rotational approach to large strain analyses. Rankin [22] introduced a procedure minimizing the square of the Euclidean norm of the local nodal displacements to obtain a formulation independent of the nodal ordering. A so-called bisector definition was used in Refs. [13, 23, 24] to define the local element frame, allowing quadrilateral shell elements invariant to nodal ordering. Battini and Pacoste [25] showed that the aforementioned invariance characteristic is important for identifying the bifurcation points of perfectly symmetric structures.

In this paper, we develop a unified co-rotational framework for beams, shells, and bricks in geometrically nonlinear analysis. The local frame is specified utilizing a unified zero-spin criterion instead of an arbitrary choice or a complex formulation independent of the nodal ordering. One modification is carried out on the definition of projector, which arises naturally from the derivative of local co-rotational element frame with respect to the global degrees of freedom. A spin matrix dependent on the choice of local element frame is introduced into the projector. As a general framework with simple expression, the pseudo vector is used to describe the large nodal rotations, avoiding special procedure for different types of elements. The instantaneous spin variable is used to yield the internal forces with high-order accuracy. To demonstrate the efficiency and accuracy of the proposed framework, several numerical examples using different elements for geometrically nonlinear analysis are tested, and compared with the results of other available solutions in references.

The outline of this paper is as follows. The element kinematics is described in the next section. In Sect. 3, the unified co-rotational framework is formulated. Several modifications are introduced into the present work, making formulations unified to employ different linear elements. In Sect. 4, a couple of numerical examples are given to verify the efficiency and accuracy of the co-rotational framework. Finally, based on the numerical results, conclusions are drawn in Sect. 5.

2. Element kinematics

A simple element undergoing a motion from its initial configuration to the current one is depicted in Fig. 1. This motion can be split into two parts, the first part is a rigid translation and rotation from its initial configuration to the rotated one, and the second part is a local deformation of the rotated configuration. Thus, rotated configuration is taken as the reference of element computation, whereas for total Lagrangian the reference is the initial configuration and for updated Lagrangian it is the converged solution of the previous increment step. The deformation with respect to the reference configuration is assumed to remain small in the co-rotational method.

As shown in Fig. 1, $\mathbf{X}, \mathbf{Y}, \mathbf{Z}$ refer to global rectangular coordinate system. An orthogonal triad $\mathbf{E}_0$ with the components of $\mathbf{e}_{i0}(i = 1, 2, 3)$ defines the orientation of local element frame in the initial configuration. The point C is chosen to be the origin of local element frame, with the position vector $\mathbf{X}_0^g$ in the global coordinates.

The translation of a typical point P with position vector $\mathbf{X}^g$

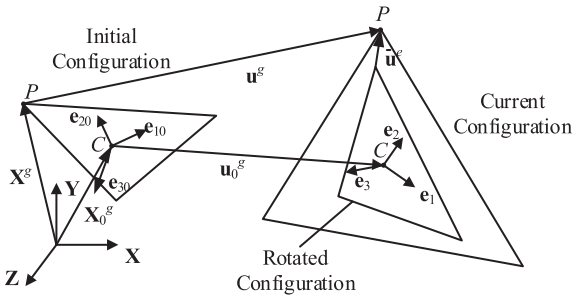

Figure 1 Element kinematics and coordinate systems.

in the global coordinates is denoted by $\mathbf{u}^g$. The superscript g denotes the quantities in global coordinate system. The position vector of this point in current configuration is written as

$$\mathbf{x}^g = \mathbf{X}^g + \mathbf{u}^g, \tag{1}$$

similarly for the origin point

$$\mathbf{x}_0^g = \mathbf{X}_0^g + \mathbf{u}_0^g, \tag{2}$$

where $\mathbf{u}_0^g$ denotes the translation of the origin point C.

The preceding local frame defined on each element is used to measure its pure deformation. The local frame in the current configuration is defined by $\mathbf{E}$ with the components of $\mathbf{e}_i (i = 1, 2, 3)$, and will be determined in Sect 3.1. The position vector of point P in the local frame is

$$\mathbf{x}^e = \mathbf{E}^{\mathrm{T}}(\mathbf{x}^g - \mathbf{x}_0^g), \tag{3}$$

where the superscript e denotes the quantities in local element frame.

Substituting Eqs. (1) and (2) into Eq. (3), the local deformational displacement of this typical point P can be written as

$$\bar{\mathbf{u}}^e = \mathbf{E}^{\mathrm{T}}(\mathbf{X}^g + \mathbf{u}^g - \mathbf{X}_0^g - \mathbf{u}_0^g) - \mathbf{X}^e, \tag{4}$$

where $\mathbf{X}^e$ is always the undeformed coordinates in local element frame, the superposed bar denotes a deformational quantity that is small in magnitude compared with its corresponding global quantity.

The global rotation of the typical point P is characterized by orthogonal matrix $\mathbf{T}^g$. This rotation matrix can be expressed by corresponding pseudo vector $\boldsymbol{\theta}^g$ with the exponential map

$$\mathbf{T}^g = \mathrm{e}^{\mathrm{spin}(\boldsymbol{\theta}^g)}, \tag{5}$$

where the notation spin$(\cdot)$ represents a skew-symmetric spin matrix as a function of the pseudo vector. Throughout the paper, we use $\mathbf{S}$ to represent the skew-symmetric matrix only for brevity.

The updating procedure from rotation $\boldsymbol{\theta}_1$ to $\boldsymbol{\theta}_2$ can be written as

$$\mathbf{T}(\boldsymbol{\theta}_2) = \mathbf{T}(\Delta\boldsymbol{\theta})\mathbf{T}(\boldsymbol{\theta}_1), \tag{6}$$

where $\Delta\boldsymbol{\theta}$ is the rotation increment, $\mathbf{T}(\cdot)$ denotes the rotation matrix of one pseudo vector, with the exponential map expression Eq. (5).

To derive the local deformational rotation, we first assume that a triad is attached to arbitrary point, such as the point P in the initial configuration, which is coincident with the initial local element frame $\mathbf{E}_0$. Therefore, this triad in the current configuration is expressed as

$$\mathbf{T} = \mathbf{T}^g\mathbf{E}_0. \tag{7}$$

This triad can be obtained in another way that the current local element frame $\mathbf{E}$ is rotated with a small rotation matrix $\bar{\mathbf{T}}^g$ in global coordinate system, such that

$$\mathbf{T} = \bar{\mathbf{T}}^g\mathbf{E}, \tag{8}$$

where the rotation matrix $\bar{\mathbf{T}}^g$ is defined by the local small rotation matrix $\bar{\mathbf{T}}^e$

$$\bar{\mathbf{T}}^g = \mathbf{E}\bar{\mathbf{T}}^e\mathbf{E}^{\mathrm{T}}. \tag{9}$$

Considering Eqs. (7)-(9), the local deformational rotation can be written in the form of rotation matrix

$$\bar{\mathbf{T}}^e = \mathbf{E}^{\mathrm{T}}\mathbf{T}^g\mathbf{E}_0. \tag{10}$$

And the corresponding local rotation $\bar{\boldsymbol{\theta}}^e$ can be obtained with the exponential map

$$\bar{\mathbf{T}}^e = \mathrm{e}^{\mathrm{spin}(\bar{\boldsymbol{\theta}}^e)}. \tag{11}$$

In accordance with Eqs. (4), (10) and (11), for a given set of global degrees of freedom, the degrees of freedom in the local element frame are obtained.

3. Modified co-rotational formulation

In this section, several improvements are introduced into the co-rotational formulation. These modifications lead to a unified formulation with higher numerical accuracy and computational efficiency for different elements.

The first modification is the specific choice of local element frame. Most work [7, 8, 17] adopt either an arbitrary choice or a complex formulation independent of the nodal ordering. A unified zero-spin criterion is proposed to choose the local element frame in present work. Consequently, the expression is unified for shell and brick elements. Using this criterion, the invariance characteristic to nodal ordering is achieved in a relatively simple manner.

The second modification concerns the projector matrix redefined in a more intuitive way. The variation of rotation matrix is expressed with instantaneous rotation variable, avoiding low-order approximation for the local rotation. During the derivation, all terms are retained, and a spin matrix is introduced, resulting in a unified formulation for different elements.

Finally, the consistent internal force and tangent stiffness are given according to these modifications. The local deformational rotation differs from the instantaneous rotation variable, thus a relatively important transformation matrix is used

to express the relationship. It is shown that different linear elements can be easily embedded into these formulations.

3.1 Unified zero-spin criterion

The local element frame shown in Fig. 1 is bound to the current deformed element configuration, and its special choice is a major issue of the co-rotational method. Zero-spin criterion is a better principle than an arbitrary choice of such a local element frame. However, most of the common procedures such as Refs. [17, 25] need to determine an in-plane rotation quantity of the local element frame by means of trigonometric function for shell elements, which makes such the option tedious and non-universal. In this work, a unified zero-spin criterion based on the polar decomposition method is proposed to address the selection with common use for 2D plate shells and 3D continua. Following this technique, the local spin at the element centroid in a current configuration is enforced to be zero, holding the local element frame invariant to the nodal ordering.

A convention in this paper that differs from the previous methods is that the origin of local frame is not placed at some element node but its centroid. This modification is consistent with the best fit criterion proposed by De Veubeke [26]. In viewpoint of numerical analysis, the deformation gradient approximation at the centroid of an element is optimally accurate. In Sect. 3.2, the derivatives of displacements at the origin are used to derive the formulation of projector. Thus such choice of the origin will also improve the numerical accuracy of the projector mapping displacements in each element from global frame to local one.

The criterion for choosing the local frame is that the local spin at the element centroid should be zero. For 3D continua, this criterion can be expressed as

$$\frac{\partial \bar{u}_2^e}{\partial X_1^e} - \frac{\partial \bar{u}_1^e}{\partial X_2^e} = 0, \tag{12}$$

$$\frac{\partial \bar{u}_2^e}{\partial X_3^e} - \frac{\partial \bar{u}_3^e}{\partial X_2^e} = 0, \tag{13}$$

$$\frac{\partial \bar{u}_3^e}{\partial X_1^e} - \frac{\partial \bar{u}_1^e}{\partial X_3^e} = 0, \tag{14}$$

where $\bar{u}_i^e (i = 1, 2, 3)$ are components of local translations, and $X_i^e (i = 1, 2, 3)$ are components of undeformed local coordinates. For 2D plate shell, this criterion can be simplified as

$$\frac{\partial \bar{u}_2^e}{\partial X_1^e} - \frac{\partial \bar{u}_1^e}{\partial X_2^e} = 0. \tag{15}$$

Figure 2 shows the process of polar decomposition, which is given as

$$\mathbf{F} = \mathbf{RU}, \tag{16}$$

where $\mathbf{U}$ denotes the symmetric right stretch matrix, and $\mathbf{R}$ is the rotation matrix.

Compared Fig. 1 with Fig. 2, it is noted that the deformation is equivalent. The former figure represents a rotation followed by a stretch while the later illustrates a process whereby the element is strained and later rotated. It is obvious that the local stretch matrix in the rotated coordinates $\mathbf{R}$ is symmetric, that means the local spin at the centroid is zero. Thus we can find the local frame in Fig. 1 by computing the rotation matrix from deformation gradient.

The previous polar decomposition is implemented to the deformation gradient in global system, and the rotation matrix can be presented as the orientation of local element frame directly. In order to apply this method to the plate shell and three-dimensional brick elements in a unified way, the present criterion takes a two-step procedure shown in Fig. 3 to specify the local element frame.

As a start, we can simply choose the initial local frame $\mathbf{E}_l$ whose origin is placed at the centroid in current configuration. The definition of this initial local frame for different elements is shown in Appendix. The initial local element frame is obviously variant to the nodal ordering and needs to be modified.

After making the first choice of local element frame, the small local nodal displacement $\mathbf{d}_l$ can be calculated according to Eq. (4). Thus the vector form of local displacement

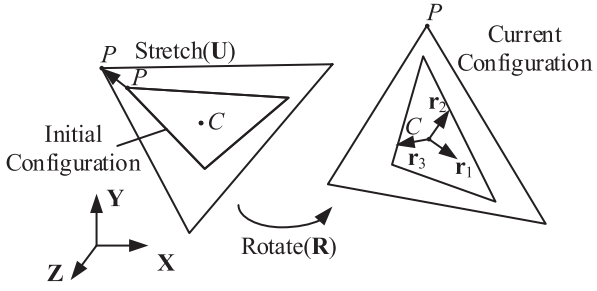

Figure 2 Polar decomposition.

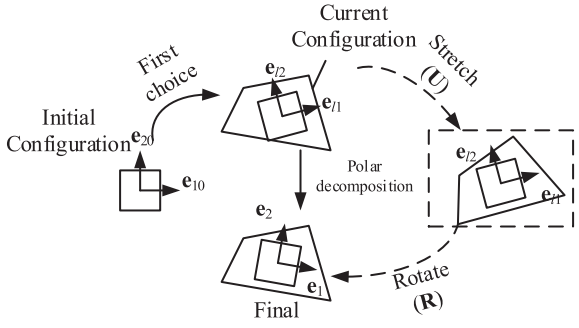

Figure 3 Two-step procedure to specify the local element frame.

gradient at the element center is then obtained

$$v(\mathbf{J}_c) = \left\{ \frac{\partial \mathbf{u}_l}{\partial \mathbf{X}^e} \right\}_c = \mathbf{B}\mathbf{d}_l, \tag{17}$$

where $v(\cdot)$ represents transforming the matrix into a vector form, $\mathbf{J}_c$ is the local displacement gradient, $\mathbf{u}_l$ represents local displacement of any point with initial local coordinates $\mathbf{X}^e$ in the element, subscript c denotes this displacement gradient is calculated at the centroid. Matrix $\mathbf{B}$ is constant obtained from conventional interpolation, independent on a particular class of element with the same connectivity. And thus the formulation is more appropriate for lower-order elements. For instance, to an eight noded brick element, the matrix $\mathbf{B}$ can be constructed by

$$\mathbf{B} = \begin{bmatrix} \mathbf{B}_1 & \cdots & \mathbf{B}_8 \end{bmatrix}, \tag{18}$$

$$\mathbf{B}_i = \begin{bmatrix} \dfrac{\partial N_i}{\partial X_1^e} & 0 & 0 & \dfrac{\partial N_i}{\partial X_2^e} & \dfrac{\partial N_i}{\partial X_3^e} & 0 & 0 & 0 & 0 \\ 0 & \dfrac{\partial N_i}{\partial X_2^e} & 0 & 0 & 0 & \dfrac{\partial N_i}{\partial X_1^e} & \dfrac{\partial N_i}{\partial X_3^e} & 0 & 0 \\ 0 & 0 & \dfrac{\partial N_i}{\partial X_3^e} & 0 & 0 & 0 & 0 & \dfrac{\partial N_i}{\partial X_1^e} & \dfrac{\partial N_i}{\partial X_2^e} \end{bmatrix}, \tag{19}$$

where $N_i (i = 1, \cdots, 8)$ are shape functions, $X_i^e (i = 1, 2, 3)$ are components of initial local coordinates.

For 2D plate shells, the local displacement gradient should be augmented to a 3×3 matrix

$$\mathbf{J}_{c3\times3} = \begin{bmatrix} \mathbf{J}_{c2\times2} & \mathbf{0}_{2\times1} \\ \mathbf{0}_{1\times2} & \mathbf{I}_{1\times1} \end{bmatrix}. \tag{20}$$

Hence, the deformation gradient of the centroid is computed as

$$\mathbf{F}_c = \mathbf{I} + \mathbf{J}_c. \tag{21}$$

Then the polar decomposition is applied to the local deformation gradient shown in Eq. (16) and the rotation matrix is obtained. This rotation matrix rotates the initial local element frame into a new frame. After this procedure, the local spin at the centroid is zero. Accordingly, the new local element frame is obtained

$$\mathbf{E} = \mathbf{R}\mathbf{E}_l. \tag{22}$$

The local displacements and rotation matrix now can be re-computed using the new local frame. When warping occurs in a quadrilateral flat shell element, this phenomenon is regarded as eccentricity and the local displacement vectors are modified according to the Ref. [13].

3.2 Derivation of the projector

A projector matrix is redefined in the present work, related to the derivative of local co-rotational element frame with respect to the global degrees of freedom. The common formulation is simplified by assuming that the finite elements are invariant under pure translation, but all the terms are retained in the present derivation. Instantaneous rotation variable is introduced to obtain the variation of a rotation matrix, being of a simple expression with higher accuracy. In particular, a spin matrix is introduced into the projector derivation.

We start with an assumption that the typical node has a virtual displacement vector $\delta\mathbf{u}^g$ in global coordinate system. The corresponding small deformation in the local element frame can be obtained by differentiating Eq. (4)

$$\delta\bar{\mathbf{u}}^e = \delta\mathbf{E}^{\mathrm{T}}(\mathbf{X}^g + \mathbf{u}^g - \mathbf{X}_0^g - \mathbf{u}_0^g) + \mathbf{E}^{\mathrm{T}}(\delta\mathbf{u}^g - \delta\mathbf{u}_0^g). \tag{23}$$

The variation of an orthogonal matrix in the above equation can be written in terms of the instantaneous axis of rotation

$$\delta\mathbf{E} = \mathbf{S}(\delta\boldsymbol{\omega}_E^g)\mathbf{E}, \tag{24}$$

where $\delta\boldsymbol{\omega}_E^g$ is the instantaneous axis of rotation for $\mathbf{E}$ in global coordinate system.

With the aid of Eq. (24) and its property, we can simplify Eq. (23) as follows:

$$\delta\bar{\mathbf{u}}^e = \mathbf{E}^{\mathrm{T}}\mathbf{S}(\Delta\mathbf{x}^g)\delta\boldsymbol{\omega}_E^g + \mathbf{E}^{\mathrm{T}}(\delta\mathbf{u}^g - \delta\mathbf{u}_0^g), \tag{25}$$

where $\Delta\mathbf{x}^g$ is the difference of current global position vector between the typical node and the origin that

$$\Delta\mathbf{x}^g = \mathbf{x}^g - \mathbf{x}_0^g. \tag{26}$$

In addition to the translational degrees of freedom, some works assume that the local rotation is reasonably small and can be obtained with low-order approximation. The variation of the rotation is then given by each component in an over-simplified way. In this work, an instantaneous rotation is introduced to yield a simple expression for the rotation with high accuracy.

The projector involved rotational part can be derived by taking the variation of Eq. (10):

$$\mathbf{S}(\delta\bar{\boldsymbol{\omega}}^e)\bar{\mathbf{T}}^e = -\mathbf{E}^{\mathrm{T}}\mathbf{S}(\delta\boldsymbol{\omega}_E^g)\mathbf{T}^g\mathbf{E}_0 + \mathbf{E}^{\mathrm{T}}\mathbf{S}(\delta\boldsymbol{\omega}^g)\mathbf{T}^g\mathbf{E}_0, \tag{27}$$

where $\delta\bar{\boldsymbol{\omega}}^e$ and $\delta\boldsymbol{\omega}^g$ are the instantaneous rotation axes in the local element frame and the global coordinates, respectively.

Substituting Eq. (10) into Eq. (27), the later equation can be written as

$$\mathbf{S}(\delta\bar{\boldsymbol{\omega}}^e) = -\mathbf{E}^{\mathrm{T}}\mathbf{S}(\delta\boldsymbol{\omega}_E^g)\mathbf{E} + \mathbf{E}^{\mathrm{T}}\mathbf{S}(\delta\boldsymbol{\omega}^g)\mathbf{E}. \tag{28}$$

According to the transformations of a vector and a tensor between the global coordinate system and the local coordinates that

$$\mathbf{r}^e = \mathbf{E}^{\mathrm{T}}\mathbf{r}^g, \quad \mathbf{S}(\mathbf{r}^e) = \mathbf{E}^{\mathrm{T}}\mathbf{S}(\mathbf{r}^g)\mathbf{E}, \tag{29}$$

Eq. (28) can be written in terms of the instantaneous rotation axis

$$\delta\bar{\boldsymbol{\omega}}^e = \mathbf{E}^{\mathrm{T}}\delta\boldsymbol{\omega}^g - \mathbf{E}^{\mathrm{T}}\delta\boldsymbol{\omega}_E^g. \tag{30}$$

For a certain element with N nodes, the projector is redefined as

$$\mathbf{P} = \frac{\delta\bar{\mathbf{v}}^e}{\delta\mathbf{v}^g}, \tag{31}$$

where $\delta\bar{\mathbf{v}}^e$ and $\delta\mathbf{v}^g$ are the node variables in the local element frame and the global coordinate system, respectively, in forms

$$\delta\bar{\mathbf{v}}^e = \left\{\delta\bar{\mathbf{u}}_1^e \ \ \delta\bar{\boldsymbol{\omega}}_1^e \ \cdots \ \delta\bar{\mathbf{u}}_N^e \ \ \delta\bar{\boldsymbol{\omega}}_N^e\right\}^{\mathrm{T}}, \tag{32}$$

$$\delta\mathbf{v}^g = \left\{\delta\mathbf{u}_1^g \ \ \delta\boldsymbol{\omega}_1^g \ \cdots \ \delta\mathbf{u}_N^g \ \ \delta\boldsymbol{\omega}_N^g\right\}^{\mathrm{T}}. \tag{33}$$

The Eqs. (25) and (30) describe the first derivatives of local degrees of freedom with respect to global ones at the typical point. Thus the relation for all nodes can be written as

$$\delta\bar{\mathbf{v}}^e = \begin{bmatrix} \mathbf{E}^{\mathrm{T}}\mathbf{S}(\Delta\mathbf{x}_1^g) \\ -\mathbf{E}^{\mathrm{T}} \\ \vdots \\ \mathbf{E}^{\mathrm{T}}\mathbf{S}(\Delta\mathbf{x}_N^g) \\ -\mathbf{E}^{\mathrm{T}} \end{bmatrix} \delta\boldsymbol{\omega}_E^g + \mathrm{diag}\left(\mathbf{E}^{\mathrm{T}}\right)(\delta\mathbf{v}^g - \delta\mathbf{u}_0^g). \tag{34}$$

Rankin and Nour-Omid [8, 9] simplify Eq. (34) by omitting the term $\delta\mathbf{u}_0^g$, assuming that the finite elements are invariant under pure translation as required by the finite element patch test. Also, they use an element node rather than the centroid as the origin in local element frame. In the present work, the origin is placed at the element centroid for the convenience of unified derivation for brick element, and all terms are retained. Hence, Eq. (34) can be further written as

$$\delta\bar{\mathbf{v}}^e = \begin{bmatrix} \mathbf{E}^{\mathrm{T}}\mathbf{S}(\Delta\mathbf{x}_1^g) \\ -\mathbf{E}^{\mathrm{T}} \\ \vdots \\ \mathbf{E}^{\mathrm{T}}\mathbf{S}(\Delta\mathbf{x}_N^g) \\ -\mathbf{E}^{\mathrm{T}} \end{bmatrix} \delta\boldsymbol{\omega}_E^g + \mathrm{diag}\left(\mathbf{E}^{\mathrm{T}}\right)\delta\mathbf{v}^g - \mathbf{N}\delta\mathbf{v}^g, \tag{35}$$

where

$$\mathbf{N} = \left[\bar{\mathbf{N}}^{\mathrm{T}}\mathbf{E} \ \ \mathbf{0} \ \cdots \ \bar{\mathbf{N}}^{\mathrm{T}}\mathbf{E} \ \ \mathbf{0}\right]^{\mathrm{T}}, \tag{36}$$

$$\bar{\mathbf{N}} = \frac{1}{N}\left[\mathbf{I} \ \mathbf{0} \ \cdots \ \mathbf{I} \ \mathbf{0}\right], \tag{37}$$

and $\mathbf{I}$ is an identity matrix.

The instantaneous axis of rotation $\delta\boldsymbol{\omega}_E^g$ in Eq. (35) is dependent on the choice of local element frame. We introduce a spin matrix that relates the instantaneous axis of rotation for local frame to the global displacements. The spin matrix ensures that the local spin at the centroid is always zero during any possible increment of motion. Accordingly,

$$\delta\boldsymbol{\omega}_E^g = \mathbf{V}\delta\mathbf{v}^g, \tag{38}$$

where $\mathbf{V}$ is the spin matrix, the detailed expressions for different elements can be seen in Appendix.

Using the expression for $\delta\boldsymbol{\omega}_E^g$ in terms of $\delta\mathbf{v}^g$, the derivative of local degrees of freedom is written as

$$\delta\bar{\mathbf{v}}^e = (\mathbf{z}^{\mathrm{T}}\mathbf{V} + \mathrm{diag}\left(\mathbf{E}^{\mathrm{T}}\right) - \mathbf{N})\delta\mathbf{v}^g, \tag{39}$$

where

$$\mathbf{z} = \left[\mathbf{z}_1 \ \cdots \ \mathbf{z}_N\right], \tag{40}$$

$$\mathbf{z}_i = \left[\left(\mathbf{E}^{\mathrm{T}}\mathbf{S}(\Delta\mathbf{x}_i^g)\right)^{\mathrm{T}} \ -\mathbf{E}\right]. \tag{41}$$

According to the Eq. (31), the projector $\mathbf{P}$ is obtained

$$\mathbf{P} = \mathbf{z}^{\mathrm{T}}\mathbf{V} + \mathrm{diag}\left(\mathbf{E}^{\mathrm{T}}\right) - \mathbf{N}. \tag{42}$$

3.3 Internal force and tangent stiffness

In order to implement the Newton-Raphson method to solve nonlinear problems, a consistent linearization is introduced to derive the internal force and tangent stiffness.

Normally, the internal force is defined as the derivative of strain energy with respect to the displacement parameters. In the local element frame, the local displacement is defined as

$$\bar{\mathbf{d}}^e = \left[\bar{\mathbf{u}}_1^e \ \ \bar{\boldsymbol{\theta}}_1^e \ \cdots \ \bar{\mathbf{u}}_N^e \ \ \bar{\boldsymbol{\theta}}_N^e\right]^{\mathrm{T}}, \tag{43}$$

where $\bar{\mathbf{u}}_i^e$ is the local translation of node i, and $\bar{\boldsymbol{\theta}}_i^e$ is the local rotation of node i.

The derivative of local rotation $\delta\bar{\boldsymbol{\theta}}^e$ in Eq. (43) is of a different nature from the instantaneous rotation $\delta\bar{\boldsymbol{\omega}}^e$. Such difference arises from the non-additive rotation increment in large rotation analysis, shown as

$$\bar{\mathbf{T}}^e(\bar{\boldsymbol{\theta}}^e + \delta\bar{\boldsymbol{\theta}}^e) = \bar{\mathbf{T}}^e(\delta\bar{\boldsymbol{\omega}}^e)\bar{\mathbf{T}}^e(\bar{\boldsymbol{\theta}}^e). \tag{44}$$

And the relationship between derivative of local rotation and instantaneous axis of rotation is given as [9, 19]

$$\frac{\partial\bar{\boldsymbol{\theta}}^e}{\partial\bar{\boldsymbol{\omega}}^e} = \mathbf{I} - \frac{1}{2}\mathbf{S}(\bar{\boldsymbol{\theta}}^e) + \eta\mathbf{S}^2(\bar{\boldsymbol{\theta}}^e), \tag{45}$$

where

$$\eta = \frac{1 - \frac{1}{2}\bar{\theta}^e \cot(\frac{1}{2}\bar{\theta}^e)}{\bar{\theta}^e}, \quad \bar{\theta}^e = |\bar{\boldsymbol{\theta}}^e|. \tag{46}$$

Then the derivative of local displacement $\delta\bar{\mathbf{d}}^e$ can be written as

$$\delta\bar{\mathbf{d}}^e = \mathbf{H}\delta\bar{\mathbf{v}}^e, \tag{47}$$

where

$$\mathbf{H} = \mathrm{diag}\left[\mathbf{I}\ \mathbf{H}_1\ \cdots\ \mathbf{I}\ \mathbf{H}_N\right], \tag{48}$$

$$\mathbf{H}_i = \frac{\partial\bar{\boldsymbol{\theta}}_i}{\partial\bar{\boldsymbol{\omega}}_i}. \tag{49}$$

Thus the relationship between the local displacement and global degrees of freedom can be expressed using the projector

$$\delta\bar{\mathbf{d}}^e = \mathbf{H}\mathbf{P}\delta\mathbf{v}^g. \tag{50}$$

Felippa and Haugen [19] point out that the **H** matrix has relative importance for tangent stiffness without the refined-mesh-limit assumption.

Under small deformation assumption in the co-rotational coordinate system, the local internal force can be given by the conventional linear relationship

$$\bar{\mathbf{f}}^e = \mathbf{K}_l\bar{\mathbf{d}}^e, \tag{51}$$

where $\mathbf{K}_l$ is the linear stiffness matrix.

Using the principle of virtual work, the global internal force is transformed from the local one

$$\mathbf{f}^g = \mathbf{P}^{\mathrm{T}}\mathbf{H}^{\mathrm{T}}\bar{\mathbf{f}}^e. \tag{52}$$

Therefore, the consistent tangent stiffness, which is defined as the variation of the internal forces with respect to global degrees of freedom, can be obtained by taking the variation of $\mathbf{f}^g$ in Eq. (52)

$$\begin{aligned}\delta\mathbf{f}^g &= \mathbf{P}^{\mathrm{T}}\mathbf{H}^{\mathrm{T}}\delta\bar{\mathbf{f}}^e + \delta\mathbf{P}^{\mathrm{T}}\mathbf{H}^{\mathrm{T}}\bar{\mathbf{f}}^e + \mathbf{P}^{\mathrm{T}}\delta\mathbf{H}^{\mathrm{T}}\bar{\mathbf{f}}^e \\ &= (\mathbf{K}_M + \mathbf{K}_P + \mathbf{K}_\theta)\delta\mathbf{v}^g \\ &= \mathbf{K}^g\delta\mathbf{v}^g.\end{aligned} \tag{53}$$

The expression of the consistent tangent stiffness $\mathbf{K}^g$ leads to three terms: the material stiffness $\mathbf{K}_M$, the projection geometric stiffness $\mathbf{K}_P$, and the moment-correction geometric stiffness $\mathbf{K}_\theta$. The detailed expressions of each term are derived in Appendix. Nour-Omid and Rankin [9] have proven that the excellent quadratic convergence can be expected when the symmetric part of the tangent stiffness matrix is used in the Newton-Raphson method for solving nonlinear equations.

According to the description of the proposed unified co-rotational framework in Sect. 2 and this section, the computational procedure relating to element quantities for geometrically nonlinear analysis can be summarized as follows.

(1) For a current configuration, use unified zero-spin criterion described in Sect. 3.1 to determine the local co-rotational coordinate system;

(2) Compute the local displacement vector according to Eqs. (4), (10) and (11). The displacement $\bar{\mathbf{d}}^e$ is assumed to be small in the local frame, thus the local internal force $\bar{\mathbf{f}}^e$can be obtained by Eq. (51);

(3) In the global coordinate system, the global internal force $\bar{\mathbf{f}}^g$ is computed using Eq. (52), and the consistent tangent stiffness $\mathbf{K}^g$ is divided into three terms as expressed by Eq. (53).

4. Numerical examples

In this section, several numerical examples are presented to demonstrate the accuracy and efficiency of the proposed co-rotational framework. In the present work, one beam element, three different shell elements, and a hexahedral element are employed in the framework for nonlinear structural analysis.

4.1 Forty-five degree curved beam

The forty-five degree curved beam involving a genuinely three-dimensional response has been tested in much work [27-30]. The geometry and material properties are shown in Fig. 4. The beam has a uniform and unit square cross-section. The beam is clamped at one end and subjected to a concentrated force at the free end. It is modeled with eight Timoshenko beam elements [20].

Table 1 compares the present solution with those given by other authors for the tip deflections at loads of 300 and 600.

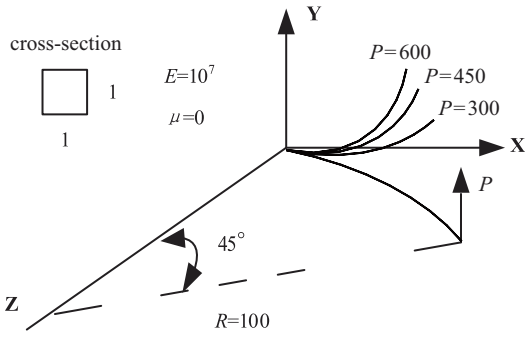

Figure 4 Forty-five degree curved beam.

Table 1 Tip deflections of various methods

Method	P=300			P=600		
	u	v	w	u	v	w
Simo et al. [27]	–11.51	39.50	–6.8	–23.51	53.40	–13.40
Bathe et al. [28]	–11.87	40.08	–6.97	–23.48	53.37	–13.51
Crisfield [29]	–12.18	40.53	–7.1	–23.87	53.71	–13.68
Ibrahimbegović et al. [30]	–	–	–	–23.70	53.50	–13.67
B31 in ABAQUS	–12.13	40.43	–7.10	–23.78	53.58	–13.62
Present	–12.14	40.47	–7.15	–23.78	53.65	–13.70

It can be seen that all methods obtain similar results and the framework proposed in the present paper is of high accuracy.

To compare with the iterative performances in other methods, we apply a sequence of three load increments of magnitude 300, 150, and 150 to the free end. Results are summarized in Table 2. It can be seen that the present solution achieves the converged results with less iterations. In addition, the present method can obtain the ultimate solution using one increment with 6 iterations, while ABAQUS cannot converge using a single increment.

4.2 Cantilever subjected to end moment

Figure 5a shows a cantilever beam subjected to end moment M at its tip. This is a classic example to exam the performance of an element undergoing large rotations.

Under the applied moment, the tip displacements are computed by the following analytical formulas:

$$\theta = \frac{ML}{EI}, w = \frac{L}{\theta}(1-\cos\theta), u = -\left(L - \frac{L}{\theta}\sin\theta\right). \tag{54}$$

In this example, the moment is $2\pi EI/L$ leading the beam rolling up into a complete circle. The beam is modeled with 16 triangular flat shell elements OTS3 [31]. Figure 5b shows the deformed configurations at some load increments. The results are attained using 16 increments with 158 iterations. Sze et al. [32] yields similar results using 16×1 S4R elements and 80 increments. The load-displacement curves at the free end are plotted in Fig. 5c, demonstrating that the present results are in good agreement with the exact solutions.

Table 2 Iterative performances (number of iterations)

Method	Load level		
	300	450	600
Simo et al. [27]	13	8	6
Bathe et al. [28]	60 equal increments		
Crisfield [29]	9	5	3
ABAQUS	12	28	
Present	6	6	5

4.3 Hemispherical shell subjected to alternating radial forces

Figure 6a shows a hemispherical shell with an 18° circular cutout at its pole. This shell is loaded by two pairs of inward and outward normal forces. Due to symmetry, only one quarter of the shell is modeled, with 16×16 four-node quadrilateral shell elements.

In this problem, we obtain the results using QTS4 [10] in 14 increments with 111 iterations. Sze et al. [32] obtained the reasonably accurate predictions using S4R element, with 27 increments and 136 iterations. Figure 6b shows the load-displacement curves. For a better insight into the size of deformation, the deformed configuration from two points of view is depicted in Fig. 6c. This hemispherical shell is a well-known example to test shell elements dealing with the warping problem that relatively large warping occurs during the analysis [13]. The numerical results are a little bit different from the reference solutions when the deformations become very large at the last equilibrium. According to Ref. [13], we modify QTS4 linear stiffness matrix with warping effect (mQTS4 in Fig. 6b) and the performance is improved. For the radial displacement at point A, the largest relative difference between mQTS4 and S4R is 0.60%, while that between QTS4 and S4R is 2.08%. The results show that the proposed co-rotational framework is efficient when warping occurs in quadrilateral shell elements.

4.4 Pinched cylindrical shell mounted over rigid diaphragms

A pinched cylindrical shell mounted over rigid diaphragms is portrayed in Fig. 7a. The cylinder is loaded by a pair of diametrically opposite point forces at the top and bottom at the midsection. Owing to symmetry, one-eighth of the cylinder is modeled with a 40×40 uniform mesh. The modified QTS4 used in the previous example is employed. The results of Ref. [32] are used as a reference for comparison. The load-displacement curves are given in Fig. 7b, and good agreement with the reference results is observed. The deformed configuration is given in Fig. 7c.

4.5 Cantilever subjected to end shear force

A cantilever subjected to end shear is shown in Fig. 8a. In the present method, we employ a symmetric hexahedral element S-MEM8S [33] into the co-rotational framework for analysis. The deformed configuration is displayed in Fig. 8b. For comparison purpose, this problem is also solved by ABAQUS C3D8I element and NASTRAN HEXA element. Sze et al. [32] solved this problem employing a mesh for

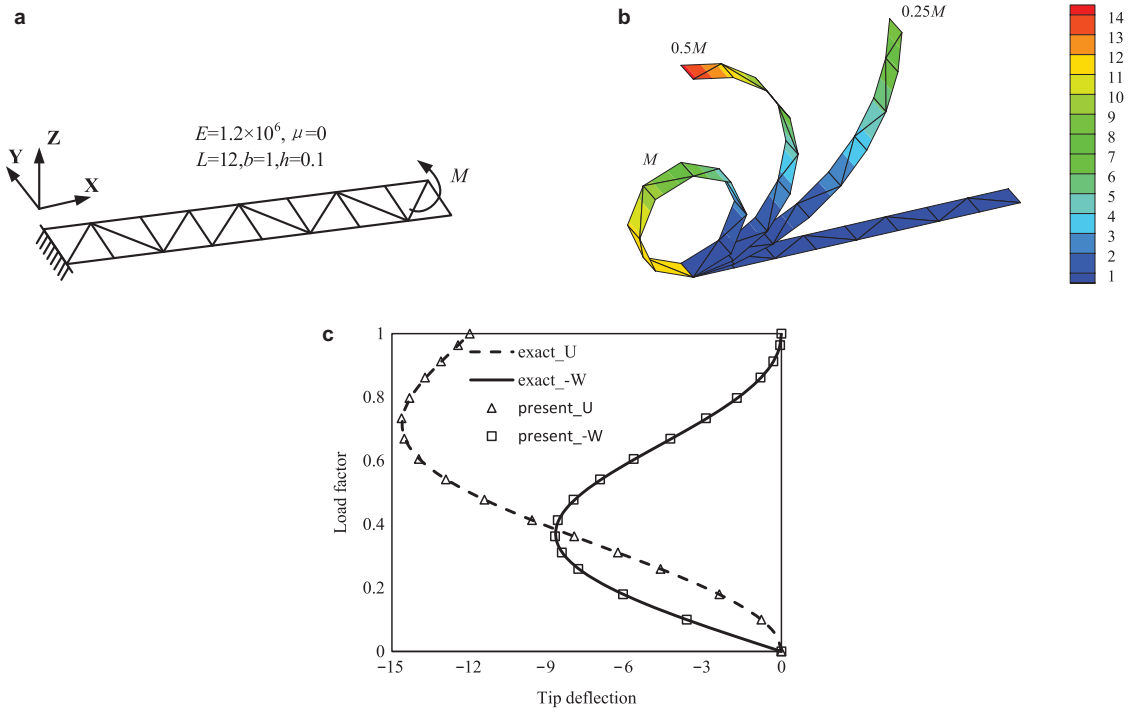

Figure 5 Cantilever beam subjected to end moment: **a** geometry and material properties; **b** deformed configurations colored by the magnitude of displacement vector; **c** load-displacement curves at the end.

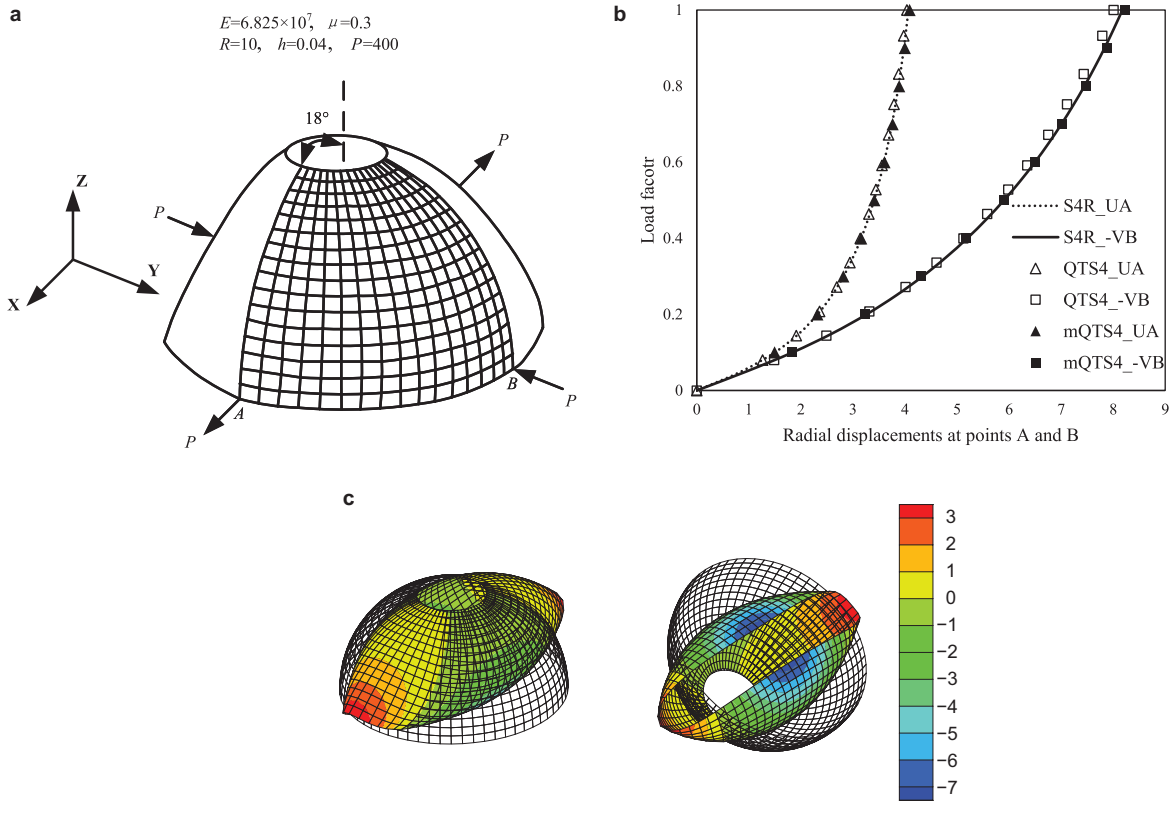

Figure 6 Hemispherical shell subjected to radial forces: **a** geometry and material properties; **b** load-displacement curves at points A and B; **c** deformed configuration colored by the radial displacement.

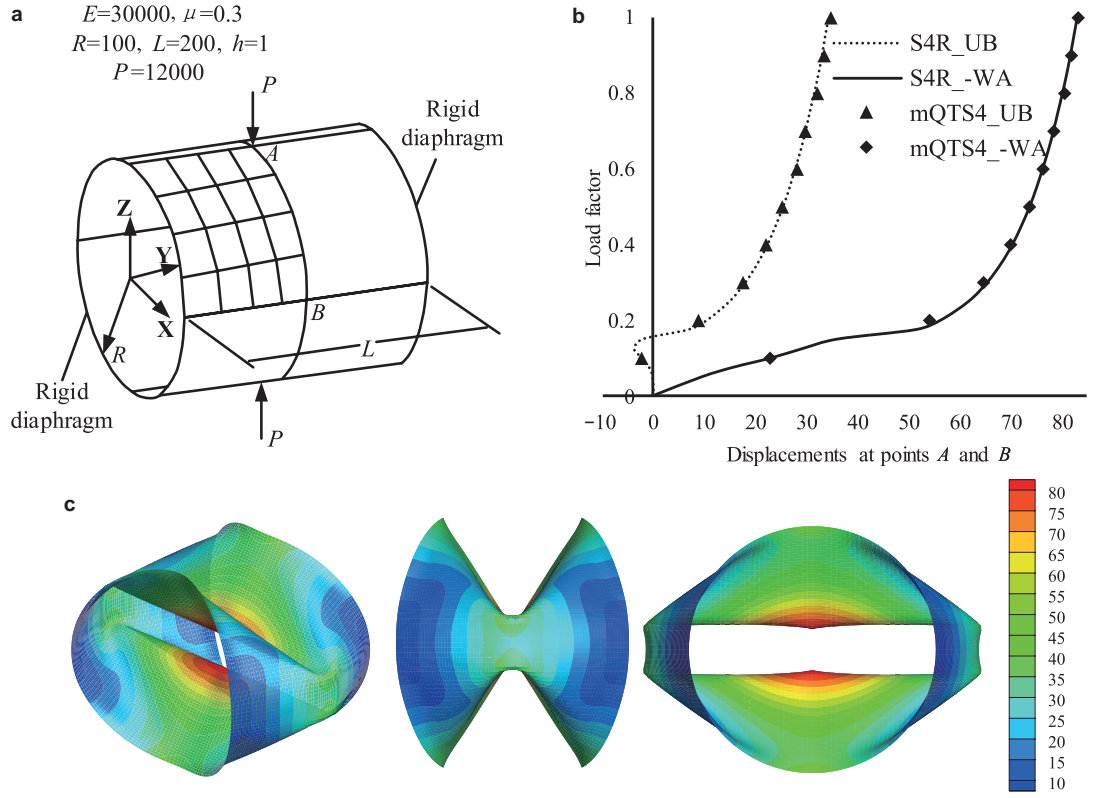

Figure 7 Pinched cylindrical shell mounted over rigid diaphragms: **a** geometry and material properties; **b** Load-displacement curves at points *A* and *B*; **c** deformed configuration colored by the magnitude of displacement vector.

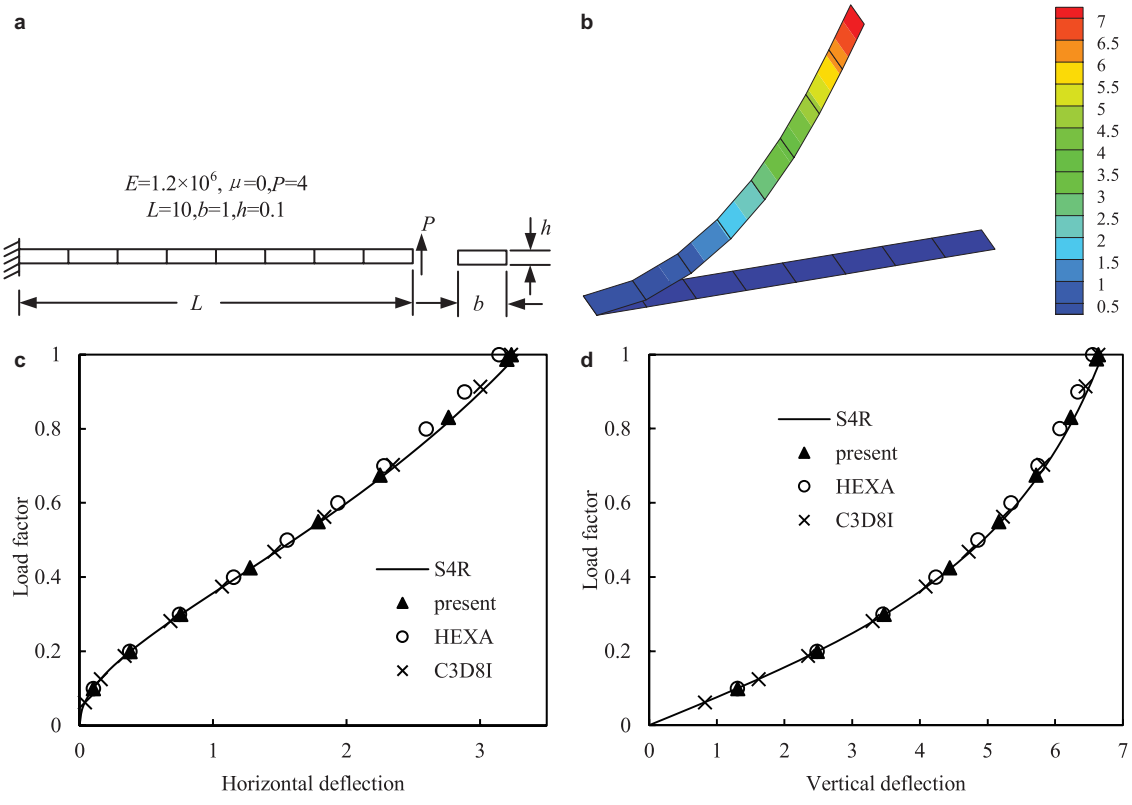

Figure 8 Cantilever subjected to end shear force: **a** geometry and material properties; **b** deformed configuration colored by the vertical displacement; **c** load versus horizontal displacement curves; **d** load versus vertical displacement curves.

S4R element . The employed mesh for the present method is 8×1 and for others is 16×1.

The results are attained using 9 increments with 43 iterations in the present method, 10 increments with 45 iterations in ABAQUS and 10 equal increments in NASTRAN. Sze et al. [32] used 15 increments and 90 iterations to obtain the results. Figure 8c and d plot the load against vertical and horizontal tip defections. It can be seen that the present co-rotational framework has excellent accuracy for brick elements. In the present method, we can also take only one increment with 7 iterations to attain the converged solutions. However, ABAQUS cannot converge in one increment, and NASTRAN leads to a less accurate result.

5. Conclusion

This paper presents a modified unified co-rotational framework for geometrically nonlinear analysis. Firstly, a unified zero-spin criterion for different elements is proposed to provide a local element frame that is invariant to the nodal ordering. The local element frame is chosen by means of polar decomposition, and its origin is placed at the centroid. Secondly, we redefine the projector matrix in a more intuitive way. A spin matrix is introduced into the derivation of projector. Thirdly, the pseudo vector and instantaneous rotation are used to deal with the accurate rotational degrees of freedom for large rotations. Within the new framework, the formulations are unified to apply linear elements for nonlinear problems. Several examples are presented in this paper, demonstrating the accuracy of the proposed co-rotational framework for a range of different types of elements.

This work was supported by the National Natural Science Foundation of China (Grant Nos. 11972297 and 11972300) and the Fundamental Research Funds for the Central Universities of China (Grant No. G2019KY05203).

1 V. A. Nguyen, M. Zehn, and D. Marinković, An efficient co-rotational fem formulation using a projector matrix, Facta Universitat. Mech. Eng. **14**, 227 (2016).
2 D. Marinkovic, M. Zehn, and G. Rama, Towards real-time simulation of deformable structures by means of co-rotational finite element formulation, Meccanica **53**, 3123 (2018).
3 Y. C. Yao, W. X. Huang, and C. X. Xu, Amplitude modulation and extreme events in turbulent channel flow, Acta Mech. Sin. **34**, 1 (2018).
4 D. Marinković, G. Rama, and M. Zehn, Abaqus implementation of a corotational piezoelectric 3-node shell element with drilling degree of freedom, Facta Universitat. Mech. Eng. **17**, 269 (2019).
5 W. L. Li, X. D. Zhi, D. Z. Wang, F. Fan, and S. Z. Shen, Influence of a roofing system on the static stability of reticulated shells, Adv. Steel Construct. **16**, 363 (2020).
6 G. Wei, Y. Jin, and L. Wu, Geometric and material nonlinearities of sandwich beams under static loads, Acta Mech. Sin. **36**, 97 (2020).
7 C. C. Rankin, and F. A. Brogan, An element independent corotational procedure for the treatment of large rotations, J. Pressure Vessel Tech. **108**, 152 (1986).
8 C. Rankin, and B. Nour-Omid, The use of projectors to improve finite element performance, Comput. Struct. **30**, 257 (1988).
9 B. Nour-Omid, and C. C. Rankin, Finite rotation analysis and consistent linearization using projectors, Comput. Methods Appl. Mech. Eng. **93**, 353 (1991).
10 Z. Wang, and Q. Sun, Corotational nonlinear analyses of laminated shell structures using a 4-node quadrilateral flat shell element with drilling stiffness, Acta Mech. Sin. **30**, 418 (2014).
11 Y. Q. Tang, Y. P. Liu, and S. L. Chan, A co-rotational framework for quadrilateral shell elements based on the pure deformational method, Adv. Steel Construct. **14**, 90 (2018).
12 Y. Q. Tang, Y. P. Liu, S. L. Chan, and E. F. Du, An innovative co-rotational pointwise equilibrating polynomial element based on Timoshenko beam theory for second-order analysis, Thin-Walled Struct. **141**, 15 (2019).
13 Y. Q. Tang, Z. H. Zhou, and S. L. Chan, A simplified co-rotational method for quadrilateral shell elements in geometrically nonlinear analysis, Int. J. Numer. Methods Eng. **112**, 1519 (2017).
14 G. F. Moita, and M. A. Crisfield, A finite element formulation for 3-d continua using the co-rotational technique, Int. J. Numer. Methods Eng. **39**, 3775 (1996).
15 M. Mostafa, M. V. Sivaselvan, and C. A. Felippa, A solid-shell corotational element based on ANDES, ANS and EAS for geometrically nonlinear structural analysis, Int. J. Numer. Methods Eng. **95**, 145 (2013).
16 H. Cho, S. J. Shin, and J. J. Yoh, Geometrically nonlinear quadratic solid/solid-shell element based on consistent corotational approach for structural analysis under prescribed motion, Int. J. Numer. Methods Eng. **112**, 434 (2017).
17 M. A. Crisfield, and G. F. Moita, A unified co-rotational framework for solids, shells and beams, Int. J. Solids Struct. **33**, 2969 (1996).
18 J. Argyris, An excursion into large rotations, Comput. Methods Appl. Mech. Eng. **32**, 85 (1982).
19 C. A. Felippa, and B. Haugen, A unified formulation of small-strain corotational finite elements: I. Theory, Comput. Methods Appl. Mech Eng. **194**, 2285 (2005).
20 Z. Wang, and Q. Sun, Stability analysis of spatial beams based on the corotational formulation, Acta Mech. Sol. Sin. **35**, 49 (2014).
21 J. M. Battini, Large rotations and nodal moments in corotational elements, Comput. Model. Eng. Sci. **33**, 1 (2008).
22 C. Rankin, On choice of best possible corotational element frame, Model. Simul. Based Eng. **1**, 772 (1998).
23 B. A. Izzuddin, An enhanced co-rotational approach for large displacement analysis of plates, Int. J. Numer. Methods Eng. **64**, 1350 (2005).
24 B. A. Izzuddin, and Y. Liang, Bisector and zero-macrospin co-rotational systems for shell elements, Int. J. Numer. Methods Eng. **105**, 286 (2016).
25 J. M. Battini, and C. Pacoste, On the choice of local element frame for corotational triangular shell elements, Commun. Numer. Methods Eng. **20**, 819 (2004).
26 B. F. De Veubeke, The dynamics of flexible bodies, Int. J. Eng. Sci. **14**, 895 (1976).
27 J. C. Simo, and L. Vu-Quoc, A three-dimensional finite-strain rod model. part II: Computational aspects, Comput. Methods Appl. Mech. Eng. **58**, 79 (1986).
28 K. J. Bathe, and S. Bolourchi, Large displacement analysis of three-dimensional beam structures, Int. J. Numer. Methods Eng. **14**, 961 (1979).
29 M. A. Crisfield, A consistent co-rotational formulation for non-linear, three-dimensional, beam-elements, Comput. Methods Appl. Mech. Eng. **81**, 131 (1990).
30 A. Ibrahimbegović, F. Frey, and I. Kožar, Computational aspects of vector-like parametrization of three-dimensional finite rotations, Int. J. Numer. Methods Eng. **38**, 3653 (1995).

31 Z. Wang, and Q. Sun, Geometrically nonlinear analysis using a corotational triangular thick and thin shell element, Eng. Mech. **31**, 27 (2014).
32 K. Y. Sze, X. H. Liu, and S. H. Lo, Popular benchmark problems for geometric nonlinear analysis of shells, Finite Elem. Anal. Des. **40**, 1551 (2004).
33 P. Q. He, Q. Sun, and K. Liang, Generalized modal element method: part-I—theory and its application to eight-node asymmetric and symmetric solid elements in linear analysis, Comput. Mech. **63**, 755 (2019).

用于梁、板壳、体单元几何非线性分析的改进的统一共旋框架

戎宇飞, 孙秦, 梁珂

摘要 共旋方法是一种近年来受到广泛关注的技术, 其可将现有的高性能线性单元扩展用于几何非线性分析. 本文提出了一种改进的梁、板壳、体单元统一的共旋框架. 提出了统一零自旋准则来确定原点始终位于单元质心的共旋坐标系. 通过引入自旋矩阵, 共旋坐标系与单元节点顺序无关. 基于共旋坐标系与全局坐标系中变量的关系, 更加直观地定义了投影矩阵. 同时, 单元转动通过伪矢量与瞬时旋转轴之间的高阶转换获得. 本文给出了统一的表达式, 以便于将一系列线性单元应用于求解框架. 给出了几个大位移分析数值算例, 结果表明本文改进的方法具有较高的效率和求解精度.